Microscopic density functional theory of wetting and drying of a solid substrate by an explicit solvent model of ionic solutions

Anna Oleksy, Jean-Pierre Hansen

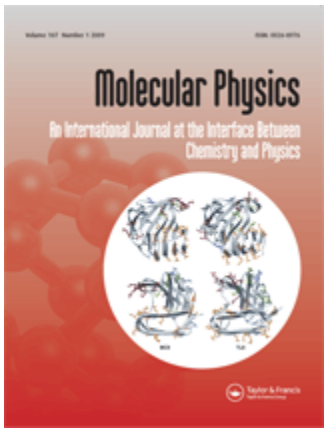

Microscopic density functional theory of wetting and drying of a solid substrate by an explicit solvent model of ionic solutions

Journal:	*Molecular Physics*
Manuscript ID:	TMPH-2009-0317.R1
Manuscript Type:	Full Paper
Date Submitted by the Author:	30-Oct-2009
Complete List of Authors:	Oleksy, Anna; University of Cambridge Hansen, Jean-Pierre; University of Cambridge
Keywords:	
Note: The following files were submitted by the author for peer review, but cannot be converted to PDF. You must view these files (e.g. movies) online.	
files.zip	

Microscopic density functional theory of wetting and drying of a solid substrate by an explicit solvent model of ionic solutions

ANNA OLEKSY and JEAN-PIERRE HANSEN
Department of Chemistry, University of Cambridge, Cambridge CB2 1EW (UK)

Abstract

Classical density functional theory (DFT) of inhomogeneous fluids is applied to an explicit solvent "semi-primitive" model (SPM) of ionic solutions to investigate the influence of ionic solutes on the wetting behaviour of a solvent in contact with a neutral or charged planar substrate. The SPM is made up of 3 species of hard sphere particles with different diameters, interacting via an attractive Yukawa potential to model excluded volume and cohesion. The solvent particles are neutral, while the monovalent anions and cations are oppositely charged. The polar nature of the solvent is modeled by a continuum dielectric permittivity linked to the local solvent density. All 3 species interact with the impenetrable substrate via an attractive external potential. While excluded volume effects are accurately described by a Rosenfeld "fundamental measure" free energy functional, the short range Yukawa attraction and Coulombic interactions are treated within the mean-field approximation. The ionic solutes are found to have a significant impact on the wetting behaviour of the solvent, in particular on the wetting temperature. Strong electric fields, or long-ranged (weakly screened) Coulombic forces are shown to have the propensity to change the wetting transition from second to first order. The cation-anion size asymmetry leads to charge separation on the liquid-vapour interface of the solution, which in turn can induce a drying transition on the liquid side of liquid-vapour coexistence.

1 Introduction.

Partial vs complete wetting of a solid substrate by a liquid in equilibrium with its vapour is a phenomenon commonly observed in every-day life, which was first quantified in 1805 by Thomas Young [1] in his famous equation relating the contact angle of a liquid drop on a planar surface to the surface tensions of the solid-liquid, solid-vapour and liquid-vapour interfaces. The existence of a surface phase transition from partial to complete wetting at a well-defined wetting temperature T_w was predicted by Cahn in 1977 [2], on the basis of a phenomenological square gradient free energy functional of the local density. Cahn predicted a first-order transition between a microscopically thin liquid film and a macroscopically thick film as the temperature T_w is crossed from below along the vapour-liquid coexistence curve. The same analysis also predicts a first-order pre-wetting transition between two liquid films of different microscopic thickness off liquid-vapour coexistence. Although Cahn only envisaged discontinuous wetting transitions, his theory can be generalised to predict the possibility of a second-order wetting transition, where the liquid film thickness diverges continuously at T_w [3]; this prediction is confirmed by more advanced Landau [4] and Landau-Ginzburg-Wilson [5] analyses. The various theoretical wetting scenarii are discussed in a number of review articles [3, 6, 7], and have been confirmed experimentally by careful ellipsometric measurements of the variation of the film thickness with temperature [8].

Whilst Cahn's theory of wetting and its extensions may be regarded as phenomenological or "mesoscopic", more microscopic density functional approaches based on explicit atomistic models were developed in parallel. Thus Ebner and Saam [9] predicted a first order transition in liquid argon films adsorbed on solid CO_2 almost simultaneously with Cahn's work, while Sullivan was the first to predict a second order wetting transition using a rather crude density functional theory (DFT) of a highly simplified microscopic model [10]. Sullivan's work was considerably extended in a seminal paper by Tarazona and Evans [11], who were the first to pinpoint the subtle relation between the order of the wetting transition and the relative ranges of the attractive interaction between the substrate and the fluid, and between the fluid atoms. They later showed that a similar DFT is capable of describing the drying of a liquid near a solid substrate, i.e. the insertion of a growing layer of vapour between the liquid and the solid ("wetting by gas") [12].

The objective of the present paper is to investigate the influence of dissolved ions on the wetting and drying behaviour of a model solvent, i.e. to study the wetting of a (charged) substrate by an ionic solution. It is well known that the interfacial properties, in particular the surface tension of a solvent, are significantly affected by the presence of a solute [13]. Hence it is to be expected that the surface phase transitions associated with wetting and drying will vary with solute concentration, and such effects may be expected to be enhanced in the case of ionic solutions, because of the formation of electric double-layers at the solid-liquid and liquid-vapour interfaces. Recently this problem was addressed by an extension of Cahn's phenomenological theory, within the "primitive model" representation of ionic solutions, which neglects the coupling between solvent molecules and ions at the molecular level [14]. In this work we apply a non-local DFT to investigate the wetting behaviour of a "semi-primitive" model of ionic solutions, introduced in an earlier paper of this series [15], which accounts for the molecular nature of the solvent. The model and the DFT formulation are presented in Section 2. The case of the pure solvent (no ions) is examined first in Section 3. The changes of interfacial properties upon adding ions are reported in Section 4. Wetting scenarii of ionic solutions near a charged substrate are derived in Section 5, while in Section 6 we show how the electric double layers formed at the interfaces strongly affect the drying behaviour of the pure solvent. Conclusions

are presented in Section 7.
While the formalism developed in this paper applies, in principle, to any electrolyte, explicit calculations are restricted to NaCl solutions.

2 Microscopic density functional formulation.

The "semi-primitive" model (SPM) of an ionic solution is made up of solvent particles (species 0), anions (species -) and cations (species +) of diameter d_α $(\alpha = 0, +, -)$. All short-range repulsive interactions are of the hard sphere type, while short-range attractive interactions are of Yukawa form. Moreover ions interact via long-range Coulombic forces. The pair potentials are hence of the generic form:

$$\mathrm{v}_{\alpha\beta}(\mathrm{r}) = \begin{cases} \infty; & \mathrm{r} < \mathrm{d}_{\alpha\beta} = (\mathrm{d}_\alpha + \mathrm{d}_\beta)/2 \\ \frac{\mathrm{q}_\alpha \mathrm{q}_\beta}{\varepsilon(\vec{r})\mathrm{r}} - \frac{\mathrm{u}}{\mathrm{r}} \exp[-\mathrm{k_f}(\mathrm{r}/\mathrm{d}_{\alpha\beta} - 1)]; & \mathrm{r} > \mathrm{d}_{\alpha\beta} \end{cases} \tag{1}$$

where $\alpha, \beta = (0, +, -)$, q_α is the electric charge of ion species α, $\varepsilon(\vec{r})$ is the local dielectric permittivity of the solvent, u is the energy scale (multiplied by unit length) of the attractive interaction, and $\mathrm{k_f}$ controls the range of this interaction. For simplicity u and $\mathrm{k_f}$ are assumed to be the same for all pairs. The model is "semi-primitive" in the sense that the interaction between solvent molecules is non-polar; for ion pairs to dissociate in such a model solvent, its polar nature must be re-introduced via a macroscopic dielectric permittivity ε, which would be constant in a bulk solution (as in the familiar "primitive model"), but is chosen to be spatially varying at interfaces, where the solvent density varies. Contrary to the case of the "primitive model", the solvent is not a mere dielectric continuum, but is atomistic in nature. As shown in our earlier work [15] and by others [16–19], this solvent granularity strongly affects the local structure of electric double-layers near charged substrates, and is hence expected to have a significant effect on wetting and drying.
Explicit calculations to be reported later were carried out for the SPM of aqueous NaCl solutions, with the following choices of diameters: $\mathrm{d}_0 = 2.80\text{Å},\ \mathrm{d}_+ = 1.90\text{Å},\ \mathrm{d}_- = 3.62\text{Å}$, while $\mathrm{q}_+ = +\mathrm{e},\ \mathrm{q}_- = -\mathrm{e},\ \mathrm{q}_0 = 0$, where e is the proton charge. The dimensionless range parameter $\mathrm{k_f}$ was chosen to be equal to 1.8 throughout (this choice gives the best fit of the Yukawa potential to a Lennard-Jones potential for $\mathrm{r} > \mathrm{d}_0$). Note that the ranges of Yukawa attractions in eq.(1) differ for each pair, since they are equal to $\mathrm{d}_{\alpha\beta}/\mathrm{k_f}$. It is convenient to introduce the following reduced temperature and densities:

$$\mathrm{T}^* = \frac{\mathrm{k_B T}}{\mathrm{u}/\mathrm{d}_0} \tag{2a}$$

$$\rho_\alpha^* = \rho_\alpha \mathrm{d}_0^3 \tag{2b}$$

where ρ_α is the number of particles of species α per unit volume. Setting aside entropic effects, wetting arises from a competition between cohesive interactions within the fluid and adhesive interactions between the fluid and the substrate. Assuming the latter to be a planar wall placed at z=0, the external potential acting on the solvent molecules and ions is chosen to be of the form:

$$\mathrm{V}_\alpha(\mathrm{z}) = \begin{cases} \infty; & \mathrm{z} < \frac{1}{2}\mathrm{d}_\alpha \\ -\mathrm{u_w} \exp(-\mathrm{k_w}(\mathrm{z}/\mathrm{d}_\alpha - 1)) - \frac{2\pi\sigma \mathrm{q}_\alpha}{\varepsilon(\mathrm{z})}\mathrm{z}; & \mathrm{z} > \frac{1}{2}\mathrm{d}_\alpha \end{cases} \tag{3}$$

where σ is the surface charge carried by the substrate, and the local dielectric permittivity of the inhomogeneous ionic solution in the vicinity of the substrate depends on the distance z>0. The exact form chosen for $\varepsilon(\mathrm{z})$ will be specified in Section 4. In the absence of ions (pure solvent) the model defined by eqs. (1) and (3) reduces to that of Tarazona and Evans [11], who showed that the ratio $\mathrm{k_f}/\mathrm{k_w}$ controls the order of the wetting transition. The reduced surface charge is defined as:

$$\sigma^* = \frac{\sigma \mathrm{d}_0^2}{\mathrm{e}} \tag{4}$$

Within DFT the key functions characterising the interfacial structure are the density profiles $\rho_\alpha(\mathrm{z})$. The fundamental order parameters are the adsorptions:

$$\Gamma_\alpha = \int_0^\infty \left[\rho_\alpha(\mathrm{z}) - \rho_\alpha^{(0)}\right] \mathrm{dz} \tag{5}$$

where the $\rho_\alpha^{(0)}$ are the bulk $(\mathrm{z} \to \infty)$ limits of the density profiles. The Γ_α can be positive (adsorption) or negative (depletion). Characteristic algebraic lengths associated with adsorbed layers may be defined by:

$$\bar{\Gamma}_\alpha = \int_0^\infty \left[\frac{\rho_\alpha(\mathrm{z})}{\rho_\alpha^{(0)}} - 1\right] \mathrm{dz} = \frac{\Gamma_\alpha}{\rho_\alpha^{(0)}} \tag{6}$$

The Γ_α are related to the surface tension γ (i.e. the surface excess grand potential per unit area) of the fluid-substrate interface by the Gibbs adsorption equation [20]:

$$\Gamma_\alpha = -\left(\frac{\partial \gamma}{\partial \mu_\alpha}\right)_{\mathrm{T},\{\mu_\beta\}} \tag{7}$$

where μ_α is the chemical potential of species α and the partial derivative is taken at fixed temperature and chemical potentials of species $\beta \neq \alpha$.
The constant equilibrium pressure throughout the interface is given by the contact theorem [20]:

$$\mathrm{P} = \mathrm{k_B T} \sum_\alpha \rho_\alpha \left(\frac{\mathrm{d}_\alpha}{2}\right) - \sum_\alpha \int_{\mathrm{d}_\alpha/2}^\infty \rho_\alpha(\mathrm{z}) \frac{\mathrm{dV}_\alpha(\mathrm{z})}{\mathrm{dz}} \mathrm{dz} \tag{8}$$

We use microscopic DFT [20] to calculate the density profiles $\rho_\alpha(\mathrm{z})$ and the surface excess grand potential of the interface which ultimately determines the wetting and drying behaviour. The key quantity is the free energy functional of the profiles $\rho_\alpha(\mathrm{z})$. This is conventionally divided into ideal ($\mathrm{F_{id}}$), hard sphere ($\mathrm{F_{HS}}$), Yukawa ($\mathrm{F_Y}$), electrostatic ($\mathrm{F_{el}}$) and correlation ($\mathrm{F_{corr}}$) contributions. The hard core correlations are contained in $\mathrm{F_{HS}}$; the remaining part of $\mathrm{F_{corr}}$, due to attractive and Coulombic interactions, is not known exactly and must be approximated, as was done in our earlier work on electric double layers [15], where it was shown that $\mathrm{F_{corr}}$ does not substantially affect the calculated profiles $\rho_\alpha(\mathrm{z})$, at least for monovalent ions. We hence set $\mathrm{F_{corr}} \equiv 0$, so that $\mathrm{F_Y}$ and $\mathrm{F_{el}}$ reduce to their mean-field expressions to be given below. An additional advantage of neglecting $\mathrm{F_{corr}}$ is that a functional containing only hard sphere (within a weighted density approximation detailed below) and mean-field contributions is thermodynamically self-consistent; this self-consistency may be spoiled

when an approximate form of $\mathrm{F_{corr}}$ is added to the functional [21]. The free energy functional per unit area hence reduces to:

$$\mathrm{F}[\{\rho_\alpha(\mathrm{z})\}] = \mathrm{F_{id}}[\{\rho_\alpha(\mathrm{z})\}] + \mathrm{F_{HS}}[\{\rho_\alpha(\mathrm{z})\}] + \mathrm{F_Y}[\{\rho_\alpha(\mathrm{z})\}] + \mathrm{F_{el}}[\{\rho_\alpha(\mathrm{z})\}] \tag{9}$$

The ideal gas contribution is known exactly:

$$\mathrm{F_{id}}[\{\rho_\alpha(\mathrm{z})\}] = \mathrm{k_B T} \sum_\alpha \int_0^\infty \mathrm{dz}\ \rho_\alpha(\mathrm{z})\{\log({\Lambda_\alpha}^3 \rho_\alpha(\mathrm{z})) - 1\} \tag{10}$$

where Λ_α is the (irrelevant) de Broglie thermal wavelength of particles of species α. For the HS contribution we choose the best available Rosenfeld functional [20, 22, 23], which is of the generic weighted density form:

$$\mathrm{F_{HS}}[\{\rho_\alpha(\mathrm{z})\}] = \int_0^\infty \mathrm{dz}\ \Phi[\{\mathrm{n_i(z)}\}] \tag{11}$$

where the free energy density Φ is a function of the weighted densities:

$$\mathrm{n_i(z)} = \sum_\alpha \int_0^\infty \mathrm{dz'}\ \rho_\alpha(\mathrm{z'}) \mathrm{w_i}^\alpha(|\mathrm{z} - \mathrm{z'}|) \tag{12}$$

The explicit form of Φ, appriopriate for a multi-component hard sphere mixture, and the weight functions $\mathrm{w_i^\alpha}$ are given in refs. [22, 23] and in the Appendix of [15].
The mean-field contribution due to the Yukawa attraction between particles is:

$$\mathrm{F_Y}[\{\rho_\alpha(\mathrm{z})\}] = \frac{1}{2} \sum_{\alpha\beta} \int_0^\infty \mathrm{dz} \int_0^\infty \mathrm{dz'} \rho_\alpha(\mathrm{z}) \mathrm{v}^{\mathrm{Y}}_{\alpha\beta}(|\mathrm{z} - \mathrm{z'}|) \rho_\beta(\mathrm{z'}) \tag{13}$$

where, using cylindrical coordinates:

$$\mathrm{v}^{\mathrm{Y}}_{\alpha\beta}(|\mathrm{z} - \mathrm{z'}|) = \int_0^{2\pi} \mathrm{d}\phi \int_{\mathrm{d}_{\alpha\beta}}^\infty \mathrm{r dr} \mathrm{v}^{\mathrm{Y}}_{\alpha\beta}(|\vec{r} - \vec{r}'|) \tag{14}$$

The mean-field electrostatic contribution reads:

$$\mathrm{F_{el}}[\{\rho_\alpha(\mathrm{z})\}] = \frac{1}{2} \int_0^\infty \mathrm{dz} \rho_\mathrm{c}(\mathrm{z}) \Psi(\mathrm{z}) \tag{15}$$

where the charge density:

$$\rho_\mathrm{c}(\mathrm{z}) = \sum_\alpha \mathrm{q}_\alpha \rho_\alpha(\mathrm{z}) \tag{16}$$

determines the electrostatic potential $\Psi(\mathrm{z})$ via Poisson's equation:

$$\frac{\mathrm{d}}{\mathrm{dz}} \left(\varepsilon(\mathrm{z}) \frac{\mathrm{d}}{\mathrm{dz}} \Psi(\mathrm{z}) \right) = -4\pi \rho_\mathrm{c}(\mathrm{z}) \tag{17}$$

which must be solved numerically for a given $\varepsilon(\mathrm{z})$ by a Runge-Kutta method, subject to the boundary conditions

$$\frac{\mathrm{d}\Psi(\mathrm{z})}{\mathrm{dz}} = -\frac{4\pi\sigma}{\varepsilon(0)}, \quad \mathrm{z}=0 \tag{18a}$$

$$\frac{\mathrm{d}\Psi(\mathrm{z})}{\mathrm{dz}} \to 0, \quad \mathrm{z}\to\infty \tag{18b}$$

Note that these boundary conditions automatically enforce the global electroneutrality condition:

$$\int_0^\infty \mathrm{dz}\rho_\mathrm{c}(\mathrm{z}) + \sigma = 0 \tag{19}$$

Eqs. (9)-(18) completely define the free energy functional used in the present work.
The equilibrium density profiles are obtained by minimising the grand potential:

$$\Omega[\{\rho_\alpha(\mathrm{z})\}] = \mathrm{F}[\{\rho_\alpha(\mathrm{z})\}] + \sum_\alpha \int \mathrm{dz}\left[\mathrm{V}_\alpha(\mathrm{z}) - \mu_\alpha\right]\rho_\alpha(\mathrm{z}) \tag{20}$$

with respect to the $\rho_\alpha(\mathrm{z})$ for fixed chemical potentials μ_α. This results in three coupled Euler-Lagrange equations which can be cast in the form:

$$\begin{aligned}\rho_\alpha(\mathrm{z}) = \rho_\alpha^{(0)} \exp\Big\{-\tfrac{1}{\mathrm{k_B T}}\Big[&\mu_\alpha^{\mathrm{HS}}[\{\rho_\beta(\mathrm{z})\}] - \mu_\alpha^{\mathrm{HS}}(\{\rho_\beta^{(0)}\}) + \mu_\alpha^{\mathrm{Y}}[\{\rho_\beta(\mathrm{z})\}] \\ &-\mu_\alpha^{\mathrm{Y}}(\{\rho_\beta^{(0)}\}) + \mathrm{q}_\alpha\Psi(\mathrm{z}) + \mathrm{V}_\alpha^{\mathrm{Y}}(\mathrm{z})\Big]\Big\}\end{aligned} \tag{21}$$

where $\rho_\alpha^{(0)} = \rho_\alpha(\mathrm{z}\to\infty)$ are the bulk densities away from the interface,

$$\mu_\alpha^{\mathrm{HS}}[\{\rho_\beta(\mathrm{z})\}] = \frac{\delta \mathrm{F}_{\mathrm{HS}}[\{\rho_\beta(\mathrm{z})\}]}{\delta\rho_\alpha(\mathrm{z})} \tag{22}$$

$$\mu_\alpha^{\mathrm{Y}}[\{\rho_\beta(\mathrm{z})\}] = \frac{\delta \mathrm{F}_{\mathrm{Y}}[\{\rho_\beta(\mathrm{z})\}]}{\delta\rho_\alpha(\mathrm{z})} = \sum_\beta \int_0^\infty \mathrm{dz}'\rho_\beta(\mathrm{z}')\mathrm{v}_{\alpha\beta}^{\mathrm{Y}}(|\mathrm{z}-\mathrm{z}'|) \tag{23}$$

and $\mu_\alpha^{\mathrm{HS}}(\{\rho_\beta^{(0)}\})$, $\mu_\alpha^{\mathrm{Y}}(\{\rho_\beta^{(0)}\})$ are the corresponding hard sphere and Yukawa contributions to the bulk chemical potentials. The implicit coupled equations (21) must be solved numerically by an iterative algorithm; at each iteration the electrostatic potential $\Psi(\mathrm{z})$ must be calculated by solving Poisson's equation (17), thus ensuring global electroneutrality at each step.

Once the profiles $\rho_\alpha(\mathrm{z})$ have converged to their equilibrium values, substitution into eq. (5) yields the adsorptions, while substitution into eq. (20) yields the grand potential (per unit area) of the total system. The surface excess grand potential Ω^{ex} and hence the surface tension is finally given by:

$$\gamma = \Omega^{\mathrm{ex}}[\{\rho_\alpha(\mathrm{z})\}] = \Omega[\{\rho_\alpha(\mathrm{z})\}] - \Omega(\{\rho_\alpha^{(0)}\}) = \mathrm{F}[\{\rho_\alpha(\mathrm{z})\}] - \mathrm{F}(\{\rho_\alpha^{(0)}\}) - \sum_\alpha \mu_\alpha\rho_\alpha^{(0)}\bar{\Gamma}_\alpha \tag{24}$$

A convenient "quality control" of the numerical procedure is provided by the Gibbs adsorption equation (7). The estimates of the adsorptions provided by eq. (5) and by differentiating the surface tension as obtained from eq. (24) with respect to μ_α are found to agree within better than 2% (cf. Table 2 of ref. [15]). A similar quality control based on the contact theorem (8) is less conclusive, because the bulk pressure $\left(\mathrm{P} = -\Omega(\{\rho_\alpha^{(0)}\})/\mathrm{V}\right)$ on the l.h.s. is a small number, while the difference on the r.h.s. is a difference of two large numbers, typically more than an order of magnitude larger than P. The numerical accuracy of the satisfaction of the two sum-rules obviously depends on the mesh size used in the integrations; a more elaborate procedure would involve a careful extrapolation to zero mesh size, which we have not attempted.

The wetting and drying transitions to be discussed in the following sections are conveniently characterised by plotting the reduced adsorptions $\Gamma_\alpha \mathrm{d}_0^2$ as functions of reduced temperature T* along the vapour-liquid coexistence curve of the SPM. Off coexistence the relevant thermodynamic field is the deviation of the Gibbs free energy per particle:

$$\mathrm{g} = \sum_\alpha \mathrm{x}_\alpha \mu_\alpha \tag{25}$$

from its value at vapour-liquid coexistence (x_α is the number concentration of particles of species α in the bulk). Prewetting and complete wetting above the wetting temperature are then characterised by monitoring the reduced adsorptions as functions of $\log(\mathrm{d}_0\Delta\mathrm{g}/\mathrm{u})$ on the vapour side (where u/d_0 is the energy scale in eq. (1)), while drying is characterised by similar plots on the liquid side of coexistence.

3 Pure solvent

We first consider the ion-free, pure solvent. For this one-component case we may drop the species indices, and refer to the model as the hard-core Yukawa (HCY) fluid, the wetting and drying behaviour of which has been extensively investigated by Tarazona and collaborators using a functional similar to the mean-field functional introduced in Section 2 [11, 12, 24]. The difference between the earlier work and ours lies in the hard sphere contribution F_{HS} to the functional (9). While Tarazona et al. used the crude local density approximation (LDA) [11], or a simple non-local, weighted density approximation [12, 24] for F_{HS}, we have used the most accurate version of the Rosenfeld "fundamental measure" hard sphere functional, which accounts for dimensional cross-over [22] (important for thin films) and reduces to the quasi-exact equation of state of Mansoori et al. [23, 25] for homogeneous hard sphere mixtures.

For an investigation of wetting and drying, the vapour-liquid coexistence curve of the HCY model needs to be known very accurately; the densities of the coexisting phases at each temperature are determined by the standard equilibrium conditions:

$$\left\{ \begin{array}{l} \mu(\rho^{(\mathrm{g})}, \mathrm{T}) = \mu(\rho^{(\mathrm{l})}, \mathrm{T}) \\ \mathrm{P}(\rho^{(\mathrm{g})}, \mathrm{T}) = \mathrm{P}(\rho^{(\mathrm{l})}, \mathrm{T}) \end{array} \right\} \tag{26}$$

In the present one-component case the equation of state of Mansoori et al. reduces to that of Carnahan

and Starling (CS); the mean-field term $\mathrm{F_Y}$ can be calculated analytically, resulting in:

$$\mu = \mu_{\mathrm{id}} + \mu_{\mathrm{CS}} + \mu_{\mathrm{Y}} = \mathrm{k_B T}\log(\Lambda^3\rho) + \mathrm{k_B T}\frac{3\eta^3 - 9\eta^2 + 8\eta}{(1-\eta)^3} - 24\frac{\mathrm{u}}{\mathrm{d}}\eta\left(\frac{1}{\mathrm{k_f}} + \frac{1}{\mathrm{k_f^2}}\right) \tag{27}$$

$$\mathrm{P} = \mathrm{P_{CS}} + \mathrm{P_Y} = \mathrm{k_B T}\rho\left[\frac{1+\eta+\eta^2-\eta^3}{(1-\eta)^3}\right] - 12\frac{\mathrm{u}}{\mathrm{d}}\rho\eta\left(\frac{1}{\mathrm{k_f}} + \frac{1}{\mathrm{k_f^2}}\right) \tag{28}$$

where $\eta = \pi\rho\mathrm{d}^3/6$ is the packing fraction, and u/d and $\mathrm{k_f}$ are the energy scale and the range parameter of the Yukawa potential (cf. eq. (1)).
The resulting phase diagram is shown in Fig. 1. The reduced critical temperature and density are $\mathrm{T_c^*} = 0.9782,\ \rho_{\mathrm{c}}^* = 0.2491$.

Our investigation of wetting, prewetting and drying transitions of the HCY model parallels that of Tarazona et al. [11, 12, 24]. The main finding of these authors is that the wetting transition in the vicinity of an attractive substrate, with a suficiently strong wall-fluid interaction defined by eq. (3) (with $\sigma = 0$), can be first or second order, depending on the ratios of the ranges and depths of the fluid-fluid and substrate-fluid interactions. Since they found no major changes in the wetting behaviour upon replacing a local HS functional [11] by a non-local one [24], it is reasonable to assume that the further upgrade to a fundamental measure Rosenfeld functional will only introduce minor quantitative corrections without changing the general trends.

The Euler-Lagrange equation (21) which must be solved to compute the equilibrium density profile reduces for the one-component HCY solvent to:

$$\rho(\mathrm{z}) = \rho^{(0)}\exp\left\{-\beta\left(\mu^{\mathrm{HS}}[\rho(\mathrm{z})] - \mu^{\mathrm{HS}}(\rho^{(0)}) + \mathrm{V^Y(z)} + \int_0^\infty \mathrm{dz'}\left(\rho(\mathrm{z'}) - \rho^{(0)}\right)\mathrm{v^Y}(|\mathrm{z}-\mathrm{z'}|)\right)\right\} \tag{29}$$

All calculations were carried out for a single value of the fluid-fluid attraction range parameter $\mathrm{k_f} = 1.8$, while the substrate-fluid range parameter was varied in the interval $0.9 \le \mathrm{k_w} \le 1.8$. The wall-fluid energy scale was chosen to be $\mathrm{u_w} = 1.75\mathrm{u}\frac{\mathrm{k_w}}{\mathrm{k_f}}$ throughout.
Typical density profiles at two temperatures and several bulk vapour densities below the coexistence density ρ_{co} are shown in Fig. 2 for $\mathrm{k_w} = \mathrm{k_f} = 1.8$. For $\mathrm{T} = 0.759\mathrm{T_c}$ the liquid film is seen to remain microscopically thin up to coexistence, while at the higher temperature $\mathrm{T} = 0.818\mathrm{T_c}$ the film thickness grows continuously as $\rho \to \rho_{\mathrm{co}}$. We are in the presence of a second-order wetting transition at a temperature $\mathrm{T_w}$ intermediate between the $0.759\mathrm{T_c}$ and $0.818\mathrm{T_c}$. The variation of the adsorption Γ with $\log(\mathrm{d}(\mu - \mu_{\mathrm{co}})/\mathrm{u})$ for several temperatures is illustrated in Fig. 3. Below the wetting temperature $\mathrm{T_w} \simeq 0.761\mathrm{T_c}$ the adsorption is seen to level off at a finite, microscopic value as coexistence is approached. For $\mathrm{T} > \mathrm{T_w}$ the adsorption diverges logarithmically. The wetting transition is hence clearly of second order and there is no sign of a prewetting transition off coexistence.

We next consider the case where the substrate-fluid attraction is of longer range than the fluid-fluid attraction, i.e. $\mathrm{k_w} = 1.2 < \mathrm{k_f} = 1.8$. In this case the profiles (not shown) exhibit a discontinuous jump in thickness before coexistence is reached along an isotherm over a limited range of temperatures above $\mathrm{T_w} \simeq 0.783\mathrm{T_c}$. The corresponding adsorption curves are plotted in Fig. 4 along six isotherms.

The prewetting transition is clearly visible in the range $0.783 \leq \mathrm{T}/\mathrm{T_c} \leq 0.818$, where the latter temperature is the prewetting critical temperature $\mathrm{T_{pwc}} \simeq 0.818\mathrm{T_c}$. The first order prewetting transition thus spans a range of only $0.025\mathrm{T_c}$. Beyond this transition the adsorption diverges logarithmically at coexistence.

4 Adding ions.

We now turn our attention to the changes to the bulk and interfacial properties of the pure solvent induced by the presence of a finite concentration of ions. The whole analysis will be carried out within the mean field density functional formalism introduced in Section 2 and applied to the pure solvent in Section 3. Focussing first on the bulk, the SPM approximately accounts for the polar nature of the solvent by the introduction of a bulk (constant) dielectric permittivity ε. Since the uniform charge density ρ_c vanishes in the bulk due to global electroneutrality, the electrostatic contribution to the total free energy of the homogeneous ionic solution is identically zero within the mean-field approximation (15). The effect of added salt on the phase diagram is hence only due to excluded volume and Yukawa attraction terms, as a consequence of the different diameters of the solvent, anion and cation species. For a given concentration c of ions in the liquid, the density of the solvent in the liquid phase of the solution and the composition of the vapour phase are calculated by imposing the following coexistence conditions, generalizing eq.(26):

$$\left\{ \begin{array}{c} \mu_0(\{\rho_\alpha^{(\mathrm{g})}\},\mathrm{T}) = \mu_0(\{\rho_\alpha^{(\mathrm{l})}\},\mathrm{T}) \\ \mu_+(\{\rho_\alpha^{(\mathrm{g})}\},\mathrm{T}) + \mu_-(\{\rho_\alpha^{(\mathrm{g})}\},\mathrm{T}) = \mu_+(\{\rho_\alpha^{(\mathrm{l})}\},\mathrm{T}) + \mu_-(\{\rho_\alpha^{(\mathrm{l})}\},\mathrm{T}) \\ \mathrm{P}(\{\rho_\alpha^{(\mathrm{g})}\},\mathrm{T}) = \mathrm{P}(\{\rho_\alpha^{(\mathrm{l})}\},\mathrm{T}) \end{array} \right\} \tag{30}$$

where we recall that the indices 0, + and - refer to solvent, cations and anions respectively. Eqs. (27) and (28), which apply to the pure solvent, must be replaced by their three-component generalizations. Thus the hard sphere contributions must be calculated from the multi-component equation of state of Mansoori et al [25], while the Yukawa contributions in eqs. (27) and (28) are generalized by the substitutions:

$$\left. \begin{array}{l} \mu_\alpha : \;\; 24\eta \;\rightarrow\; 4\pi \sum_\beta \rho_\beta \mathrm{d}_{\alpha\beta}^3 \\ \mathrm{P} : \;\; 12\rho\eta \;\rightarrow\; 2\pi \sum_{\alpha\beta} \rho_\alpha \rho_\beta \mathrm{d}_{\alpha\beta}^3 \end{array} \right\} \tag{31}$$

The resulting phase diagrams for several values of the NaCl concentration c are plotted in Fig. 1 in the (ρ_0, T) plane. The liquid-vapour coexistence curve, and in particular the critical point, is seen to be shifted to lower solvent densities as the ion concentration increases, whereas the total packing fraction of the solution is practically independent of c, as one might expect, with the exception of the critical point and its vicinity (see the inset of Fig. 1). As a consequence of the vanishing electrostatic contribution to the bulk free energy, the model solution's vapour contains substantially more ions than the amount seen in real systems, which is usually too small to detect. However, for most temperatures the salt concentration in the gas phase remains relatively low, and rises rapidly when $\mathrm{T_c}$ is approached.

Electrostatic interactions, which have no effect in the bulk within the mean-field approximation, come into play as soon as the solution is no longer homogeneous, i.e. at (planar) interfaces, characterized by density profiles $\rho_\alpha(\mathrm{z})$. Under those conditions a local dielectric permittivity $\varepsilon(\mathrm{z})$ of the solvent

must be introduced within the SPM description. We have used three approximations for $\varepsilon(\mathrm{z})$:

a) $\varepsilon(\mathrm{z}) \equiv \varepsilon$, i.e. a constant value throughout the inhomogeneous system

b) $\varepsilon(\mathrm{z})$ determined by a weighted solvent density through a local Clausius-Mossotti (CM) expression:

$$\varepsilon(\mathrm{z}) = \frac{\frac{8\pi}{9\mathrm{k_B T}}\mathrm{m}^2\tilde{\rho}_0(\mathrm{z}) + 1}{\frac{4\pi}{9\mathrm{k_B T}}\mathrm{m}^2\tilde{\rho}_0(\mathrm{z}) - 1} \tag{32}$$

where m is the dipole moment of the solvent molecules, while $\tilde{\rho}_0(\mathrm{z})$ is the local density averaged over a sphere of diameter d_0 centred at $\vec{r} = (0, 0, \mathrm{z})$:

$$\begin{aligned}\tilde{\rho}_0(\mathrm{z}) = \tfrac{6}{\pi \mathrm{d}_0^3} \int \mathrm{d}\vec{r}\,' \rho_0(\vec{r}\,')\Theta(\mathrm{d}_0/2 - |\vec{r} - \vec{r}\,'|) = \\ \tfrac{6}{\pi \mathrm{d}_0^3} \int_{-\infty}^{\infty} \mathrm{d}\mathrm{z}\,' \rho_0(\mathrm{z}\,') \left[\mathrm{d}_0^2/4 - (\mathrm{z} - \mathrm{z}\,')^2\right] \Theta\left(\mathrm{d}_0/2 - |\mathrm{z} - \mathrm{z}\,'|\right)\end{aligned} \tag{33}$$

c) A phenomenological approach whereby $\varepsilon(\mathrm{z})$ is chosen to be a sigmoidal function of the local solvent density:

$$\varepsilon(\mathrm{z}) = 1 + \frac{\mathrm{f(T)}}{1 + \exp\left[-\mathrm{a}(\tilde{\rho}_0(\mathrm{z})\mathrm{d}_0^3 - \rho_{0\mathrm{m}}(\mathrm{T})\mathrm{d}_0^3)\right]} \tag{34}$$

where $\tilde{\rho}_0(\mathrm{z})$ is defined in eq.(33), while $\rho_{0\mathrm{m}}(\mathrm{T}) = \frac{1}{2}(\rho_0^{(\mathrm{g})}(\mathrm{T}) + \rho_0^{(\mathrm{l})}(\mathrm{T}))$ is the mid-point density between the bulk densities of the gas and liquid phases coexisting at temperature T. The dimensionless parameter a, which defines the width of the sigmoid, is set equal to 40. This choice yields a permittivity profile which is not too steep or too broad across the vapour-liquid interface. The temperature-dependent function f(T) is parametrized to reproduce the dielectric permittivity of water. Assuming the reduced temperature T*=0.75 of the HSY model of the solvent to correspond to 300K and T*=0.82 to 325K, the model's wetting transitions examined in Section 3 lie between $0^{\circ}\mathrm{C}$ (T*=0.68) and $50^{\circ}\mathrm{C}$ (T*=0.82). Within this range of temperatures, the experimental permittivity data for water can be approximated by the linear function:

$$\varepsilon(\mathrm{T}) = 88 - 0.37\mathrm{T} \tag{35}$$

if temperatures are expressed in centigrades. Hence f(T) must be chosen as f(T)=87-0.37T.

Note that the CM approximation (32), which results from a mean-field description of a genuine polar fluid, leads to the familiar "dielectric catastrophe" at high density, and must hence be restricted to sufficiently small dipole moments m. Throughout our calculations we set $\mathrm{m}^* = \mathrm{m}\sqrt{\frac{1}{\mathrm{ud}_0^2}} = 0.75$, which yields ε values between 5 and 10 in the liquid. For water $\mathrm{m}^* \approx 2$, which lies outside the range where the MF approximation for dipolar interactions remains valid. The phenomenological form (34) does not suffer from such a limitation.

As all elements of the model solution are now defined, the properties of its liquid/vapour interface can be investigated. The interfacial density profiles of the three species are obtained by solving a system comprising the Euler-Lagrange (21) and Poisson's (17) equations, however with boundary conditions different from those imposed on fluids in contact with a solid substrate. We assume the asymptotic behaviour of $\rho_\alpha(\mathrm{z})$ to be:

$$\rho_\alpha(\mathrm{z}) \;\rightarrow\; \rho_\alpha^{(\mathrm{g})}; \quad \mathrm{z} \;\rightarrow\; -\infty \tag{36a}$$

$$\rho_\alpha(\mathrm{z}) \rightarrow \rho_\alpha^{(\mathrm{l})}; \quad \mathrm{z} \rightarrow \infty \tag{36b}$$

Additionally the solvent density profile is pinned at z=0, so that $\rho_0(0) = \frac{1}{2}\left(\rho_0^{(\mathrm{l})} + \rho_0^{(\mathrm{g})}\right)$. Due to size asymmetry one cannot assume that the ion profiles also have midpoints at z=0, therefore they are constrained only by (36a) and (36b). The boundary conditions imposed on the electrostatic potential are:

$$\frac{\mathrm{d}\Psi(\mathrm{z})}{\mathrm{dz}} \rightarrow 0, \quad |\mathrm{z}| \rightarrow \infty \tag{37}$$

They are equivalent to the following global electroneutrality condition:

$$\int_{-\infty}^{\infty} \mathrm{dz}\rho_\mathrm{c}(\mathrm{z}) = 0 \tag{38}$$

Two examples of the interfacial structure formed by the model solution are shown in Fig. 5. Both systems have the same solute concentration (0.1M), but differ in the approximation used for the dielectric permittivity. In the main frame the density profiles of the ions are plotted, while the insets illustrate the variation of the solvent density (almost identical for the two solutions) and of $\varepsilon(\mathrm{z})$ across the liquid-vapour interface. It is clear that the cation and anion distributions differ significantly. The ion size asymmetry causes local charge separation on the surface dividing the two phases in contact. This behaviour contrasts sharply with results obtained for symmetric electrolytes, like the restricted primitive model (composed of two ionic species equal in diameter) discussed in [26], where the charge density profile across the liquid-vapour interface vanishes identically. The magnitude of the charge separation in our system depends on the salt concentration and the dielectric permittivity of the solvent (see figures 5 and also 6, which shows the charge distribution in the system). These two parameters also define the width of the region where local electroneutrality is violated. The relation between this lengthscale, also known as the Debye length, and the ionic solution properties was estimated within the Debye-Hückel theory framework:

$$\lambda_\mathrm{D} = \sqrt{\frac{\varepsilon}{4\pi\beta\sum_\alpha \rho_\alpha \mathrm{q}_\alpha^2}} \tag{39}$$

showing that λ_D is proportional to $\sqrt{\frac{\varepsilon}{\mathrm{c}}}$. However, regardless of any variation in c or ε the liquid-vapour interface of our model NaCl solution always remains negatively charged. The differences in the cation and anion density profiles also affect the electrostatic potential across the interfacial area, as shown in the inset of Fig. 6. The local charge separation results in a potential difference $\Delta\mathrm{V}$ developing between the bulk liquid and vapour phases. $\Delta\mathrm{V}$ was found to be independent of the salt concentration or the dielectric permittivity of the solvent. Computer simulations of asymmetric primitive electrolytes [27] suggest that the gap in Ψ strongly depends on the discrepancies in the ionic radii, and increases with growing anion to cation size ratio.

Despite the crude, mean-field treatment of the coulombic interactions in the current DFT, our predictions for the electrostatic properties of the liquid-vapour surface of NaCl solutions are in good agreement with results obtained by other methods. Molecular dynamics (MD) simulations of sodium halides in water have shown that the anions (except F^-) are more abundant in the interfacial region than the cations, and that this disproportion increases with the anion's size [28, 29]. These authors concluded that the concentration of Cl^- on the surface is roughly the same as in the bulk, a feature which is also observed in our model. The findings of the MD studies were directly confirmed

by electron spectroscopy measurements [30] showing that aqueous solutions of halides indeed have negatively charged interfaces. Likewise, our results for the electrostatic potential profile are in accord with data obtained in experiments investigating the electrokinetic behaviour of air bubbles in electrolytes [31] for NaCl solutions of low pH, in which OH^- ions do not contribute to $\Psi(z)$.

5 Wetting scenarii for NaCl solutions.

Let us now consider our model solution's vapour in contact with a solid substrate exerting external potential (3) on the fluid particles. The exponential interaction parameters u_w and k_w are assumed to be the same for all species. Note that the equality of the dimensionless k_w means the actual range of the substrate-fluid attraction is the shortest for Na^+ and the longest for Cl^-. The value of the depth parameter u_w is fixed as in Section 3. It is not surprising that systems defined in this way form liquid films, just as the ion-free solvent's vapour does. Examples of such structures are shown in figures 7 and 8. The effects of the size asymmetry of the three species on the oscillatory behaviour of their density profiles at solid surfaces are discussed in detail in our earlier work [15]. Here we would like to direct attention to the influence of screening of the coulombic forces on the charge distribution in thick liquid layers. In the 1M NaCl solution pictured in Fig. 7 the counterions highly outnumber the coions only in the vicinity of the electrode, while at 0.1M concentration (Fig. 8), as the effective range of the electrostatic interactions is longer, significant charge separation is seen over the entire width of the film. Similar differences in ionic profiles are observed when systems of different dielectric permittivity were compared. The lengthscale at which local electroneutrality is violated is found to be smallest for $\varepsilon \equiv 1$ and largest for the sigmoidal function (34), as expected.

As in one-component HCY fluids, the formation of thick liquid films in NaCl solutions is associated with wetting transitions. However, the temperatures and orders of these phenomena are not necessarily the same as in the pure solvent, and may be modified by the presence of the solute and the electric field of the substrate. In this work we investigate the influence of salt concentration, surface charge density and the solvent's dielectric permittivity on the wetting behaviour of systems where k_w is 1.2, 1.8 or 1.73. The latter exponential attraction induces a second order transition in the HCY fluid ($T_w \simeq 0.753 T_c$). However, this point of the $\{u_w; k_w\}$ parameter space lies very close to the line dividing continuous and discontinuous scenarii. The wetting behaviour of the NaCl solutions was determined in the same way as for the pure solvent, by examining the density profiles of the species along the coexistence line (gas branch) and along isotherms above the estimated T_w. The results of the calculations are shown in graphic form in figures 9 and 10. The numerical values of wetting temperatures in solutions with sigmoidal permittivity are collected in Table 1.

Even when the substrate is neutral, the presence of the solute is seen to cause small, but noticeable shifts in T_w. The addition of salt generally increases the wetting temperatures; the effect is larger in concentrated than in dilute solutions, and for continuous rather than for discontinuous transitions. However, in the system with the weakest screening of the coulombic forces among the solutions considered, T_w is found to be slightly lower than in the pure solvent, most likely due to an increase in the overall fluid-fluid interaction range.

Introducing the surface charge strengthens the interaction between the substrate and the solute. If the wetting transition in the underlying HCY fluid is first order, the relation between σ and T_w of the SPM solution is straightforward - the larger $|\sigma|$ is, the lower T_w. The $T_w(|\sigma|)$ relation is seen to be roughly linear for both positively and negatively charged substrates. For $\varepsilon(z) = \text{constant}$ (not shown) T_w is consistently slightly higher if $\sigma < 0$ and sodium cations are the counterions. It is most likely a result

of the differences in the ranges of the Yukawa interactions - chlorine ions are the biggest species in the system and have the longest attraction range, both with other particles and with the wall. Under conditions for which the wetting transition is second order the influence of the substrate charge density follows a different pattern. The impact of the σ sign inversion on $\mathrm{T_w}$ is now comparable with that of changing $|\sigma|$ by a factor of 2, and the transition temperature is higher if $\sigma > 0$. The linear character of the $\mathrm{T_w}(|\sigma|)$ relation is disrupted for critical transitions near positively charged substrates, with a maximum appearing for moderate σ. Apparently the accumulation of big anions, which promotes the formation of a wetting film in a discontinuous process, interferes with the steady growth of a liquid layer, consisting mainly of smaller solvent 'molecules'. An increase in NaCl concentration causes an upward shift in the transition temperatures, as in the case of systems at a neutral wall. Higher salt content results in stronger screening of the electrostatic forces, which makes wetting less favourable. The dielectric permittivity influences wetting in two ways. Switching ε from 1 to 80 substantially increases the effective range of the coulombic interactions, but at the same time reduces their strength. As a result systems with $\varepsilon \equiv 1$ generally have a lower $\mathrm{T_w}$ than systems where ε is high in the liquid. However, a very large Debye length can cancel out the effect of smaller interparticle forces and shift $\mathrm{T_w}$ downwards.

It transpires that the order of the wetting transition does not change with the addition of ions over a wide range of parameters considered. However, it is clear that a sufficiently strong external electric field can turn a continuous process into a discontinuous one. Just what constitutes a 'sufficiently strong' field depends on the properties of the fluid, in particular the two quantities which influence the lengthscale of the coulombic forces, namely c and ε. In a 0.1M NaCl solution with a Clausius-Mossotti dielectric permittivity function the change in order occurs only for high substrate charge densities of $\sigma > 0.55\,\mathrm{e/nm^2}$ (or $|\sigma| > 1.11\,\mathrm{e/nm^2}$ if the wall is negatively charged). If $\varepsilon(\mathrm{z})$ is replaced by the sigmoidal expression, while the other parameters defining the system remain unchanged, the second to first order shift is much easier to induce, and takes place at low to moderate σ. We have also observed that wetting becomes discontinuous for weaker external electric fields if the larger anions are the counterions. This result is most likely due to the difference in ranges of ion-substrate and ion-solvent exponential interactions involving $\mathrm{Na^+}$ and $\mathrm{Cl^-}$ species.

6 Drying phenomena in the SPM

The hard core Yukawa fluid dries completely in contact with a hard wall ($\mathrm{u_w} = 0$ throughout this section) for any temperature, and since its particles are neutral, adding substrate surface charge alone cannot modify this dewetting scenario. However, when salt is introduced into the system, the solution's drying behaviour is found to be profoundly modified due to the attractive interactions between the electrode and the counterions.

Let us first consider a positively charged wall. Fig. 11 shows a representative example of an electric double layer formed by our SPM in contact with such a substrate. Although the liquid is under conditions corresponding to a state on the liquid-vapour coexistence line, the density profiles exhibit only limited depletion. Unlike for the underlying HCY fluid no complete drying occurs. The integrated charge density profile $\mathrm{I_c(z)}$

$$\mathrm{I_c(z)} = \sigma + \int_0^{\mathrm{z}} \mathrm{d}z'\rho_{\mathrm{c}}(\mathrm{z}') \tag{40}$$

plotted in the inset of Fig. 11 provides an explaination of this phenomenon. It is clear that the first layer of chlorine anions does not fully neutralise the substrate, and a net amount of positive charge remains at the solid-fluid interface. On the other hand the liquid-vapour interface of our SPM NaCl solution is negatively charged. The two interfaces attract each other, and hinder drying. We have observed the same effect in all systems with $\sigma > 0$ which we have investigated. Fig. 12 shows the variation of the solvent adsorption Γ_0 as a function of σ, while all parameters describing the solution are constant (the system is under liquid-vapour coexistence conditions). The adsorptions of the ionic components follow curves similar in shape, but different in absolute values. For positively charged substrates Γ_0, which is a measure of depletion in the system, remains finite, and continuously diverges as $\sigma \to 0$ (if the wall is neutral complete drying occurs).

One instantly notices the asymmetry w. r. t. the sign inversion of σ. For negatively charged model electrodes Γ_0 is finite only up to a certain threshold surface charge density. If $|\sigma|$ is smaller than this value, the substrate becomes completely dry, i.e. $\Gamma_0 \to -\infty$. Like the drying hindrance associated with $\sigma > 0$, this phenomenon can be understood as a consequence of the distribution of ions in the inhomogeneous system. A typical example of the structure formed by our model NaCl solution near a negatively charged wall (partially wet state) is shown in Fig. 13. Despite adsorbing a layer of Na^+ counterions, the substrate is still seen to carry residual negative charge. Therefore, the solid-fluid and liquid-vapour interfaces are now like-charged. In such a system drying can only be hindered if σ is so large that the Yukawa attraction from the adsorbed cations outweighs the solvent cohesion forces and (if there is sufficient depletion for the liquid-vapour interface to start forming) electrostatic repulsion between the two surfaces.

Instead of varying σ for one thermodynamic state of the liquid branch of the liquid-vapour coexistence line one can choose to move along the coexistence curve while keeping the substrate's electric field constant. After performing such calculations we have noticed that there is a certain temperature below which the wall is partially wet, and above which it is completely dry. In other words, unlike the pure solvent, for which the contact angle $\theta = 180°$ along the entire liquid-vapour coexistence line, the ionic solution undergoes a drying transition at a temperature $\mathrm{T_d}$. From Fig. 12 we can conclude that for 1M NaCl in a solvent described by the CM permittivity function, and $\sigma = -0.90\,\mathrm{e/nm^2}$, $\mathrm{T_d} \simeq 0.769\mathrm{T_c}$. The relation between the drying temperature and surface charge density was found to display a trend opposite to the one observed for $\mathrm{T_w}$, since $\mathrm{T_d}$ increases with growing $|\sigma|$. The dielectric permittvity in the liquid has no apparent effect on $\mathrm{T_d}$. The drying temperatures are the same for solutions differing only by the approximation for $\varepsilon(\mathrm{z})$, namely the CM function (32) or the sigmoidal expression (34). We have also analysed the behaviour of adsorption upon varying the distance from the liquid-vapour coexistence line along isotherms, and found that for all systems we have investigated, if a drying transition occurs, it is first order. Given the nature of the process, we speculate that it is unlikely to be continuous for any combination of parameters defining interactions in the solution for which $\mathrm{T_d} < \mathrm{T_c}$; the special case of $\mathrm{T_d} = \mathrm{T_c}$ would require a separate investigation.

7 Discussion and conclusions

We have examined the influence of ionic solutes on the wetting and drying behaviour of model fluids close to their liquid-vapour equilibrium, in contact with a planar charged substrate. The model ionic solution is based on an expicit solvent representation, which fully accounts for excluded volume effects, contrary to the familiar "primitive model", but not for the polar nature of the solvent

molecules, which is approximately taken care of by the introduction of a local dielectric permittivity ("semi-primitive model"). In a further step towards physical reality, different hard core diameters are assigned to the three species (solvent, anions and cations), a refinement which we have shown to have a significant incidence on wetting and drying scenarios.

Our DFT analysis of interfacial phenomena of ionic solutions begins with the re-examination of the wetting behaviour of the HCY solvent to provide an ion-free benchmark against which the effects of ionic solutes and external electric fields are measured. The pure solvent results are in qualitative agreement with earlier studies [11, 12, 24], but some quantitative differences are observed, due to our use of a more accurate density functional for the hard sphere contribution to the free energy. The next step has been to quantify the influence of the ionic solutes on the structure of the electrolyte-electrode interface, and on the order and location of the surface phase transitions. The physical parameters which were varied are, apart from the temperature, the NaCl salt concentration, the surface charge density σ of the substrate and the dielectric permittivity of the model solvent. Concerning the wetting transitions, the most common effect we found upon adding salt is a drop in the wetting temperature $\mathrm{T_w}$, amounting to about 3% or less, under most conditions which were investigated. This drop is generally found to be a monotonically decreasing, linear function of $|\sigma|$. This trend can be explained quite straightforwardly - charging up the substrate strenghtens the substrate-fluid attraction (counterion-substrate directly, and solvent-substrate indirectly), and the transition temperature shifts downwards accordingly, just as for one-component fluids. However, some of the solutions examined in this work are exceptions to this rule - the $\mathrm{T_w}(|\sigma|)$ function was found to display a maximum for moderate wall charge densities. It shows that in multi-component fluids increasing the attraction between the solid and just one ingredient of the mixture may not lead to a lower transition temperature, and that the constituents may compete in forming the wetting film. When systems differing only in salt concentration were compared, the one with a higher solute content was always found to have a higher $\mathrm{T_w}$. It indicates that the range of the electrostatic interactions is a factor of considerable importance for the location of the wetting transition. The analysis of the influence of the third parameter defining the charge-charge forces - the dielectric permittivity - yields results consistent with this conclusion. No universal trends linking $\mathrm{T_w}$ and ε were found, which is not surprising as increasing the dielectric permittivity increases the range of electrostatic interactions (which makes wetting more favourable), but on the other hand decreases their strength (which is a hindrance to liquid film formation). However, in systems with the largest Debye length, where the charge separation is not limited to the vicinity of the electrode, but spans the whole width of the wetting film, the increment in range is seen to outweigh the reduction in the substrate-counterion attraction.

The order of the wetting transition in most systems containing ions was found to be the same as in the corresponding solute-free fluids. However, several cases of a cross-over from a continuous to a discontinuous process caused by electrostatic forces were observed. In systems with a short Debye length, where the counterion excess extends over only one layer, a transition which was second order in the ion-free solvent may become first order if the solution is placed in contact with a highly charged substrate. By contrast, if the solution is based on the same HCY fluid, but is characterised by long-ranged Coulombic forces (charge separation spanning the entire liquid film width) discontinuous wetting is found even for moderate $|\sigma|$ values. Additionally, the change in the wetting temperature accompanying the change in scenario is much larger than in any other system with comparable charge density on the substrate. The problem of the influence of ionic solutes on the order of surface phase transitions has been considered earlier by Denesyuk and Hansen [14], although in their model the solvent particles were not taken into account explicitly, and their free energy was approximated by a

phenomenological Cahn-type functional. The current study concurs with the conclusion reached in the earlier analysis that long-ranged electrostatic interactions favour first-order wetting. Both works also agree that, when Coulombic forces are strongly screened, the type of transition in a salt solution tends to be the same as in the pure solvent. However, the investigation in reference [14] did not predict the connection between high substrate surface charge density and an inclination towards discontinuous wetting, which is observed in the current study. This discrepancy is a consequence of the different level of accuracy of the fluid structure description in the respective solution models. The preference for a first order wetting transition in systems with high $|\sigma|$, which has been observed in the work presented in this paper, stems from interactions involving the layers formed on the substrate's surface by the counterions and the solvent. The calculations in [14] do not account for the layering phenomena, and therefore overlook their influence on wetting. Similarly, the solute-induced switch from a first order to a critical transition predicted in [14] is not likely to occur for a solution which incorporates an explicit solvent. The authors of the earlier work found such a scenario in systems with medium ion concentration and moderate to high wall surface charge density. The current analysis, however, shows that substrates possessing the latter characteristic favour first order wetting. Likewise, we found no evidence of a sequence of two wetting transitions, predicted in [14] for some salt solutions in the region of the parameter space adjacent to that where the cross-over from a discontinuous to a continuous transition takes place. The scenario cannot be completely ruled out, since the fraction of the parameter space explored in our study is much smaller than in [14] due to the much larger computational effort needed to determine the transition characteristics in a system where all three species are considered on a microscopic level. However, the layering effects certainly limit the extent of conditions under which such a sequential process is possible.

The drying phenomena which occur on the liquid side of the liquid-vapour coexistence curve are less frequently discussed in the literature. However, the model considered here displays some very interesting behaviour in this region. The solute-free HCY liquid dries completely in contact with a hard wall for any temperature between the triple and the critical point, which is typical of a one-component fluid. When ions and surface charge on the substrate are added the drying behaviour of the system changes radically. The interaction between the wall and the counterions gives rise to an effective solid-fluid attraction, which hinders complete drying. Depending on the sign of the substrate's charge, the contact angle may remain below 180° for any temperature, or a drying transition may occur. While the former scenario is quite common, the latter is rarely observed in semi-infinite vapour/liquid/solid systems, and usually associated with discountinuous interaction potentials (e.g. square well [32–34], truncated Lennard-Jones [35–37]). It is however not out of the ordinary in fluids of elongated particles, where an intrusion of an isotropic phase between the wall and a nematic phase is called drying [38, 39], or in liquids under confinement (capillary evaporation). The drying behaviour of our model is determined by the interaction between the solid-fluid (substrate with adsorbed counterions) and liquid-vapour interfaces, which may be attractive (making complete drying impossible) or repulsive (phase transition possible). When a drying transition does occur, it was found to be first order. The relation between its characteristic temperature $(\mathrm{T_d})$ and $|\sigma|$ is of opposite trend to the case of $\mathrm{T_w}$.

In our earlier work [15] we discussed asymmetry-specific phenomena caused by realistic cation-anion size ratios in systems composed of ionic solutions and a hard sphere solvent. Predictably, the wetting transitions in the current model are affected as well. The wetting temperatures were found not to be equal in systems differing only by the sign of σ. Interestingly, the trend of the difference depends on the order of the transition. If the process is discontinuous, it occurs between a very thin film consisting mainly of the counterions, and a completely wet state. In this situation the counterion

with the longest range of exponential attraction (chlorine) induces wetting at a lower temperature. For the same reason the transition changes order from second to first more easily if anions are attracted to the wall. On the other hand, in critical wetting the film growth passes through all the intermediate length scales, so that steric competition between the solvent and the ions becomes important. This results in lower $\mathrm{T_w}$ for substrates attracting small sodium cations. If the dielectric permittivty of the solvent is inhomogeneous its variation also contributes to the wetting temperature asymmetry with respect to the sign reversal of σ, since ε is then different for each ion type at a distance $\mathrm{d}_\alpha/2$ from the substrate (higher for anions). Such a local increase in ε weakens the attraction between the solid and the first layer of counterions, and hence the influence of introducing a nonuniform permittivity function can be expressed by the inequality $\Delta\mathrm{T_w}(+|\sigma|) > \Delta\mathrm{T_w}(-|\sigma|)$. The aforementioned exceptions, where $\mathrm{T_w}(|\sigma|)$ is not a monotonically decreasing function, are systems in which the hard core repulsion between the solvent and adsorbed chlorine and the modification of electrostatic forces by inhomogeneous dielectric permittivity both work towards increasing $\mathrm{T_w}$. There is another interesting disparity in the way the transitions of different order are affected by ion size asymmetry. First order wetting temperatures depend mainly on the absolute value of the substrate surface charge density, and the sign of σ has a relatively small influence. In critical wetting the sign reversal has a more significant impact on $\mathrm{T_w}$, comparable with varying $|\sigma|$ by a factor of 2. It indicates that the location of a discontinuous transition depends chiefly on the substrate-fluid potential, while for a continuous transition the details of both substrate-fluid and fluid-fluid interactions have a significant influence on $\mathrm{T_w}$.

The impact of ion size asymmetry on drying behaviour is even more profound than on wetting. If a substrate-solution exponential attraction is absent, it is the sign of the charge density on the wall which determines what surface phase transition scenarios are available to the system. Two factors contribute to this outcome. The first is the charge distribution at the free liquid-vapour interface of the model solution. Due to unequal cation and anion diameters the density profiles of the two species are not identical and $\mathrm{Cl^-}$ ions were found to be more abundant at the interface. This feature has been observed experimentally [30] - electron spectroscopy experiments have shown that aqueous solutions of halides have negatively charged surfaces. The second factor is the incomplete screenig of the substrate's electric field by the first layer of monovalent counterions. Therefore, if σ is positive the solid-fluid interface still carries a residual positive charge, despite the adsorbed anions. In this situation, even if the direct substrate-solution interaction is weak and vapour intrudes between the two phases, the interfaces bordering this third entity will attract each other and limit the gas film thickness to finite values. It is the only drying scenario available for systems with $\sigma > 0$. However, if σ is negative the intruding vapour is confined by interfaces that repel each other, leading to a contact angle of $180°$. As vapour entry between the solid and the liquid is more likely at higher temperatures, a drying transition may occur. Of course scenarios where either a completely or partially dry state persists for all $\mathrm{T_t} < \mathrm{T} < \mathrm{T_c}$ are also possible.The results may be different for multivalent cations like $\mathrm{Ca^{2+}}$, which show charge inversion, i.e. the charge of the first cation layer is higher than σ. However, to account for this effect a density functional beyond the level of the MF approximation would have to be used for the electrostatic contribution to the free energy. The first order drying transition is predicted to occur in the absence of any long-range wall-fluid dispersion attraction. If the latter were included, the predicted drying transition may well be suppressed. Further work will be required to investigate the competion between wall-fluid Coulombic and dispersion forces regarding a possible drying transition.

The least attractive aspect of the "semi-primitive model" considered in the present paper is the use of a

non-polar solvent and the phenomenological introduction of an inhomogeneous continuum dielectric permittivity. A more satisfactory model must include a solvent of dipolar particles. DFT calculations of the wetting and drying behaviour of ionic solutions based on such a fully microscopic model will be reported in a subsequent publication.

Acknowledgements

The authors are grateful to P. Bryk, R. Evans and R. Roth for helpful discussions. AO acknowledges the financial support of the Cambridge European Trust, Corpus Christi College Cambridge, Schlumberger Cambridge Research and the EPSRC.

References

[1] T. Young. Phil. Trans. R. Soc. London **95**, 63 (1805).

[2] J. W. Cahn. J. Chem. Phys. **66**, 3667 (1977).

[3] P. G. de Gennes. Rev. Mod. Phys. **57**, 827 (1985).

[4] H. Nakanishi and M. E. Fisher. Phys. Rev. Lett. **49**, 1565 (1982).

[5] E. Brézin, B. I. Halperin, and S. Leibler. J. Physique (Paris) **44**, 775 (1983).
E. Brézin, B. I. Halperin, and S. Leibler. Phys. Rev. Lett. **50**, 1387 (1983).

[6] S. Dietrich. in *Phase Transitions and Critical Phenomena*, C. Domb and J. L. Lebowitz, editors, volume 12. Academic Press, London (1988).

[7] M. Schick. in *Liquids at Interfaces*, J. Charvolin, J. F. Joanny, and J. Zinn-Justin, editors. North Holland, Amsterdam (1990).

[8] D. Bonn and D. Ross. Rep. Progr. Phys. **64**, 1085 (2001).

[9] C. Ebner and W. F. Saam. Phys. Rev. Lett. **38**, 1486 (1977).

[10] D. E. Sullivan. Phys. Rev. B **20**, 3991 (1979).
D. E. Sullivan. J. Chem. Phys. **74**, 2604 (1981).

[11] P. Tarazona and R. Evans. Mol. Phys. **48**, 799 (1983).

[12] P. Tarazona and R. Evans. Mol. Phys. **52**, 847 (1984).

[13] Y. Levin and J. E. Flores-Mena. Europhys. Lett. **56**, 187 (2001).

[14] N. A. Denesyuk and J.-P. Hansen. J. Chem. Phys. **121**, 3613 (2004).

[15] A. Oleksy and J.-P. Hansen. Mol. Phys. **104**, 2871 (2006).

[16] M. J. Grimson and G. Rickayzen. Chem. Phys. Lett. **86**, 71 (1982).

[17] Z. Tang, L. E. Scriven, and H. T. Davis. J. Chem. Phys. **100**, 4527 (1994).

[18] L. J. Douglas Frink and F. van Swol. J. Chem. Phys. **105**, 2884 (1996).

[19] L. Lamperski, C. W. Outhwaite, and L. B. Bhuiyan. Mol. Phys. **87**, 1049 (1996).

[20] J.-P. Hansen and I. R. McDonald. *Theory of Simple Liquids*. Academic Press, Amsterdam, 3rd edition, (2006). Chap. 6.

[21] M. B. Sweatman. Mol. Phys. **98**, 573 (2000).

[22] Y. Rosenfeld, M. Schmidt, H. Löwen, and P. Tarazona. Phys. Rev. E **55**, 4245 (1997).

[23] R. Roth, R. Evans, A. Lang, and G. Kahl. J. Phys. Cond. Matter **14**, 12063 (2002).

[24] P. Tarazona, U. Marini Bettolo Marconi, and R. Evans. Mol. Phys. **60**, 573 (1987).

[25] G. A. Mansoori, N. F. Carnahan, K. E. Starling, and T. W. Leland Jr. J. Chem. Phys. **54**, 1523 (1971).

[26] B. Groh, R. Evans, and S. Dietrich. Phys. Rev. E **57**, 6944 (1998).

[27] F. Bresme, M. González-Melchor, and J. Alejandre. J. Phys. Cond. Matter **17**, S3301 (2005).

[28] P. Jungwirth and D. J. Tobias. J. Phys. Chem. B **105**, 10468 (2001).

[29] P. Jungwirth and D. J. Tobias. J. Phys. Chem. B **106**, 6361 (2002).

[30] S. Ghosal, J. C. Hemminger, H. Bluhm, B. S. Mun, E. L. D. Hebenstreit, G. Ketteler, D. F. Ogletree, F. G. Requejo, and M. Salmeron. Science **307**, 563 (2005).

[31] C. Li and P. Somasundaran. J. Colloid Interface Sci. **146**, 215 (1991).

[32] F. van Swol and J. R. Henderson. Phys. Rev. A **43**, 2932 (1991).

[33] F. van Swol and J. R. Henderson. Phys. Rev. A **40**, 2567 (1989).

[34] P. Bryk, A. Patrykiejew, and S. Sokoł owski. Phys. Chem. Chem. Phys. **2**, 3227 (2000).

[35] E. Velasco and P. Tarazona. J. Chem. Phys. **91**, 7916 (1989).

[36] F. van Swol and J. R. Henderson. J. Phys. Cond. Matter **2**, 4537 (1990).

[37] M. J. P. Nijmeijer, C. Bruin, A. F. Bakker, and J. M. J. van Leeuwen. Phys. Rev. B **44**, 834 (1991).

[38] K. Shundyak and R. van Roij. Europhys. Lett. **74**, 1039 (2006).

[39] M. Bier, L. Harnau, and S. Dietrich. J. Chem. Phys. **125**, 184704 (2006).

σ [e/nm^2]	$k_w = 1.2$				$k_w = 1.8$			
	c=0.1M		c=1M		c=0.1M		c=1M	
	T_w/T_c	order	T_w/T_c	order	T_w/T_c	order	T_w/T_c	order
0.00	0.782	1st	0.785	1st	0.760	2nd	0.765	2nd
+0.28	0.771	1st	0.782	1st	0.743	1st	0.770	2nd
-0.28	0.774	1st	0.782	1st	0.742	2nd	0.759	2nd
+0.55	0.760	1st	0.773	1st	0.733	1st	0.768	2nd
-0.55	0.765	1st	0.774	1st	0.726	1st	0.750	2nd

Table 1: Wetting transitions of the semi-primitive model of NaCl in water. The concentrations c refer to the salt content in the liquid. The dielectric permittivity $\varepsilon(z)$ is approximated by the sigmoidal function (34).

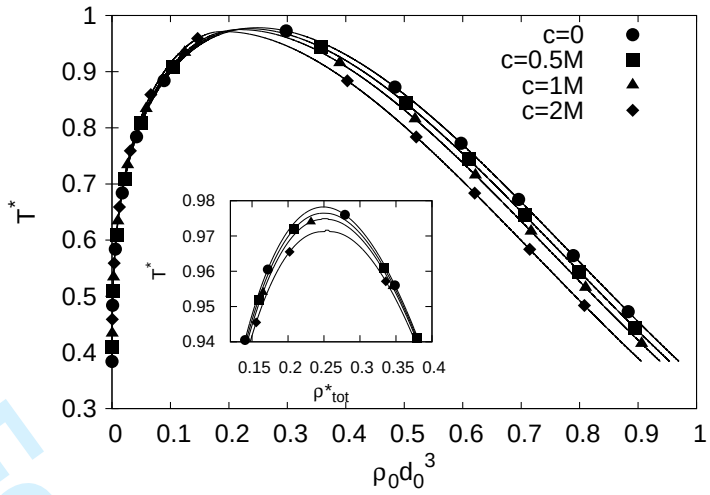

Figure 1: The solvent densities $\rho_0^* = \rho_0 \mathrm{d}_0^3$ of coexisting liquid and vapour phases as a function of temperature and NaCl concentration (symbols). The inset shows the total density - temperature phase diagrams near the critical point.

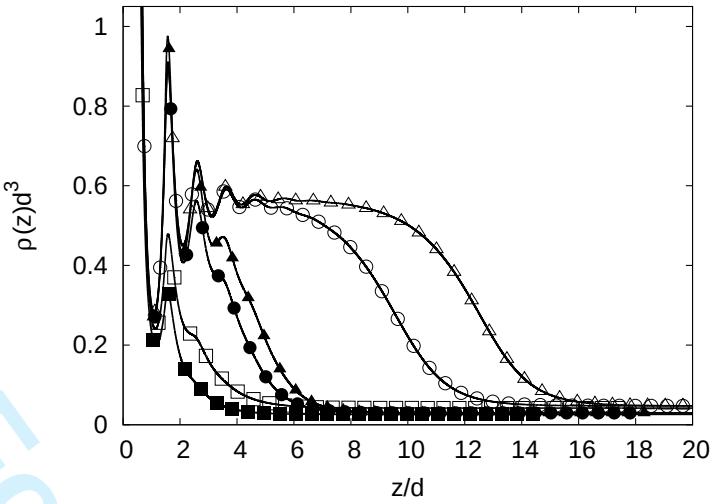

Figure 2: Density profiles of the pure HCY solvent vs distance z from the planar substrate. The lines with full symbols correspond to $0.759\mathrm{T_c}$, and lines with empty symbols to $0.818\mathrm{T_c}$. The shape of the symbols indicates the distance from coexistence - the profiles at $0.9\rho_{\mathrm{co}}$ are marked with squares, at $0.999\rho_{\mathrm{co}}$ with circles and at $0.99995\rho_{\mathrm{co}}$ with triangles.

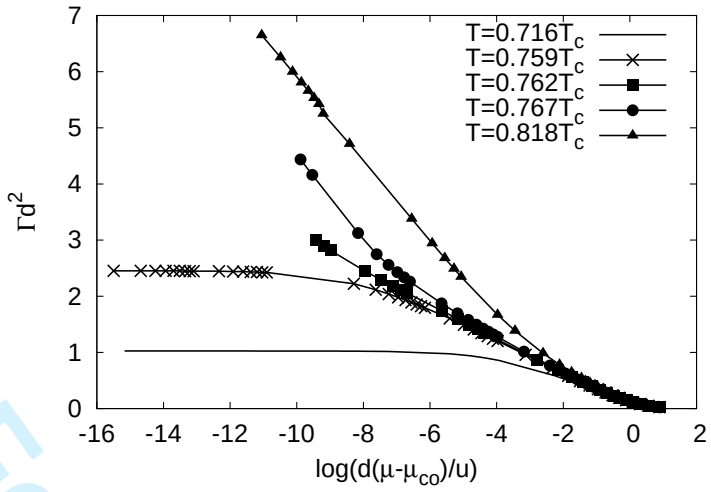

Figure 3: Adsorption of the HCY fluid as a function of distance from coexistence along five isotherms for dimensionless inverse range parameters $k_w = k_f = 1.8$.

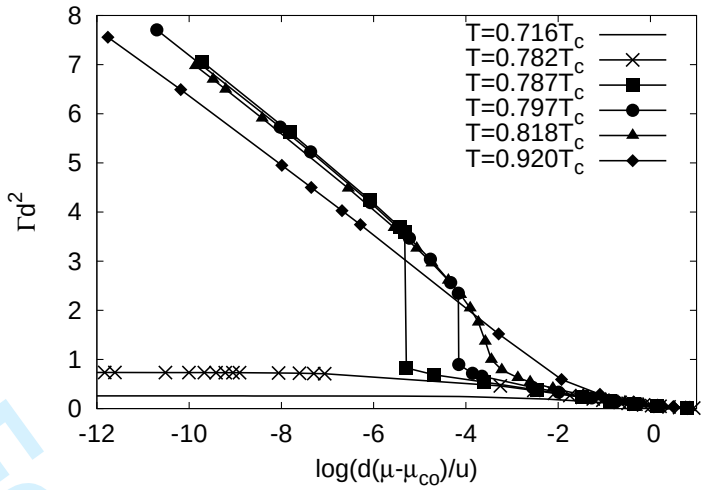

Figure 4: Same as in Fig. 3, but for $k_w = 1.2$, $k_f = 1.8$ and six isotherms.

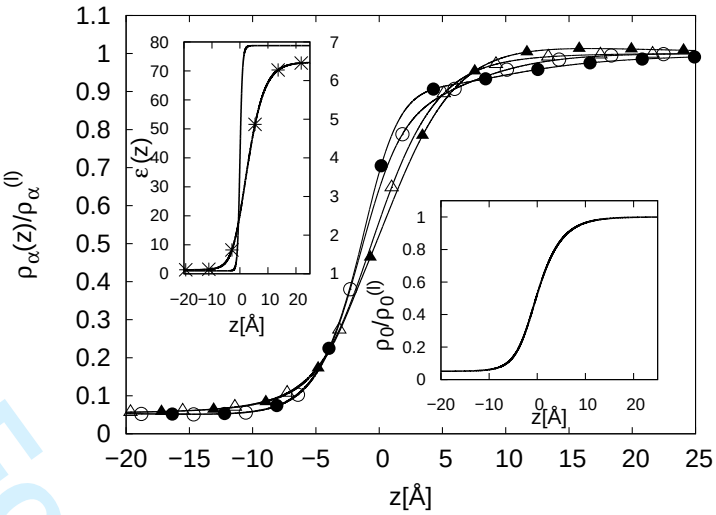

Figure 5: Density profiles of the ions across the liquid-vapour interfaces of two SPM models of a 0.1M NaCl solution at $T^* = 0.75(298K)$. The two models differ by the solvent dielectric permittivity - filled symbols indicate $\varepsilon(z)$ given by (34), and empty symbols mean that the CM expression (32) is used. Lines with circles correspond to chlorine anions and lines with triangles to sodium cations. The inset in the bottom right corner shows the solvent density profile (only one is plotted as there are no significant differences between the models). In the upper left corner the permittivity functions are displayed. The line with crosses and the right-hand y axis corresponds to the CM approximation, while the plain line and the left-hand y axis corresponds to the sigmoidal expression.

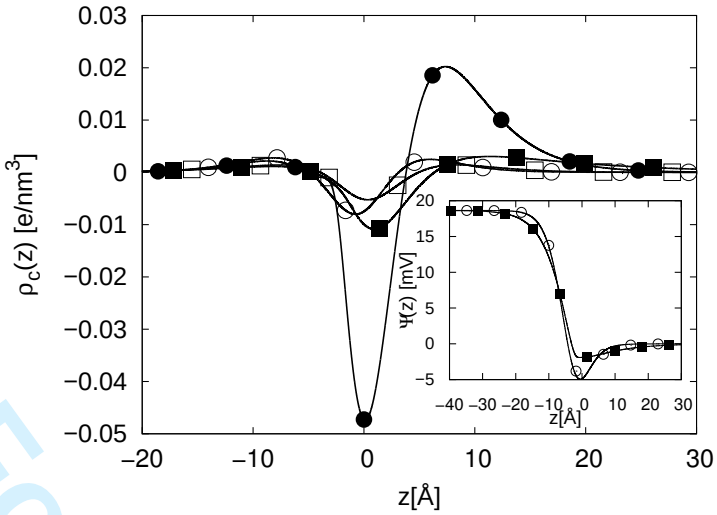

Figure 6: Charge density profiles across the liquid-vapour interface of NaCl solutions. The shape of the symbols distinguishes between different concentrations - circles for 1M and squares for 0.1M. Filled symbols correspond to sigmoidal permittivity, while empty ones to the CM $\varepsilon(z)$. Electrostatic potential profiles are shown in the inset for two of the four solutions.

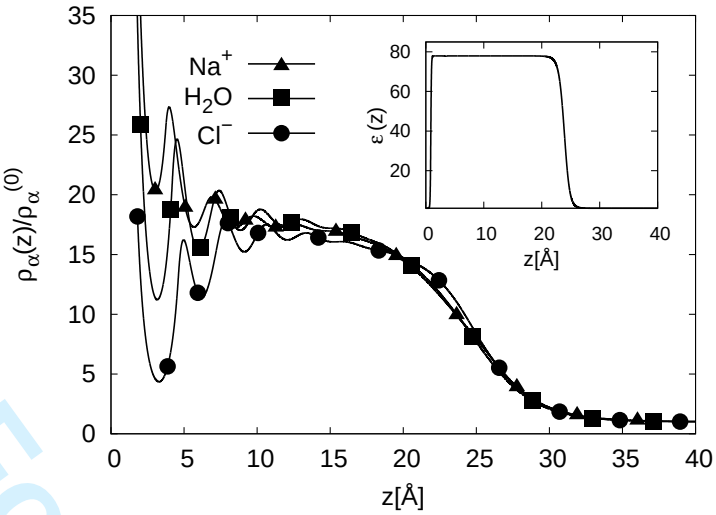

Figure 7: Density profiles $\rho_\alpha(\mathrm{z})$ of a liquid film formed by NaCl vapour at $\rho = 0.999\rho_{\mathrm{co}}$ (the saturated vapour coexists with a 1M solution) at a charged substrate. $\varepsilon(\mathrm{z})$ is sigmoidal, $\mathrm{k_w} = 1.2$, $\sigma = -0.55\,\mathrm{e/nm^2}$, $\mathrm{T} = 0.775\mathrm{T_c}$. The inset shows the dielectric permittivity profile.

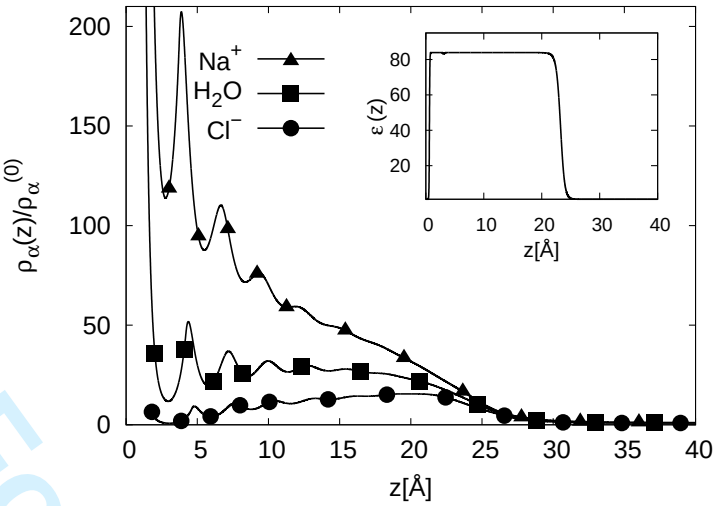

Figure 8: Density profiles of NaCl vapour at $\rho = 0.9999\rho_{\mathrm{co}}$ (the saturated vapour coexists with an 0.1M solution) at a charged substrate. $\varepsilon(\mathrm{z})$ is sigmoidal, $\mathrm{k_w} = 1.8,\ \ \sigma = -0.55\,\mathrm{e/nm^2},\ \ \mathrm{T} = 0.727\mathrm{T_c}$. The inset shows the dielectric permittivity profile.

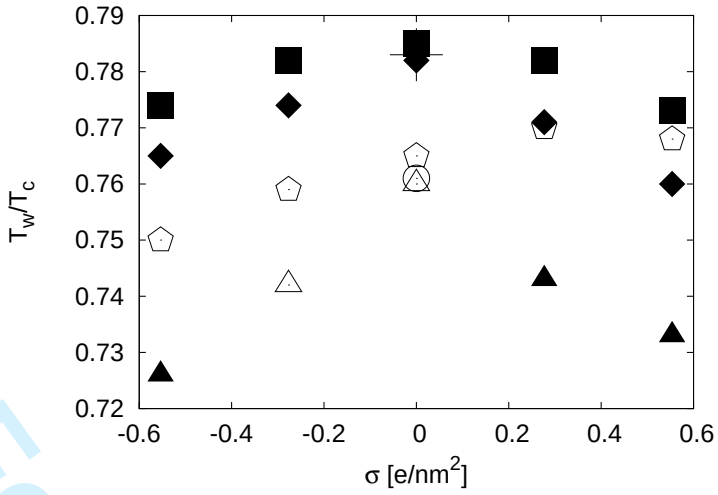

Figure 9: Wetting temperatures of SPM NaCl solutions with sigmoidal permittivity as a function of substrate surface charge density. The symbols correspond to the following $\{k_w; c\}$ pairs: ⬠ $\sim \{1.8; 1M\}$; △ $\sim \{1.8; 0.1M\}$; □ $\sim \{1.2; 1M\}$; ♢ $\sim \{1.2; 0.1M\}$; ◯ $\sim \{1.8; 0\}$. A filled symbol signifies a first order transition, while an empty one a second order transition. The location of the transition in the pure HCY fluid near a substrate with $k_w = 1.2$ is marked with a '+'.

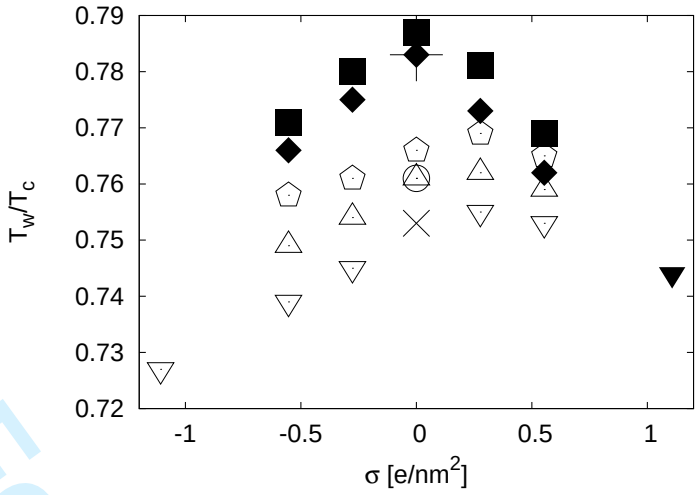

Figure 10: Same as in Fig. 9, but for solutions with Clausius-Mossotti permittivity. The symbol code is as in Fig. 9, with the additional ∇ symbol corresponding to a $\{1.73; 0.1\mathrm{M}\}$ system, and $\times \sim \{1.73; 0\}$.

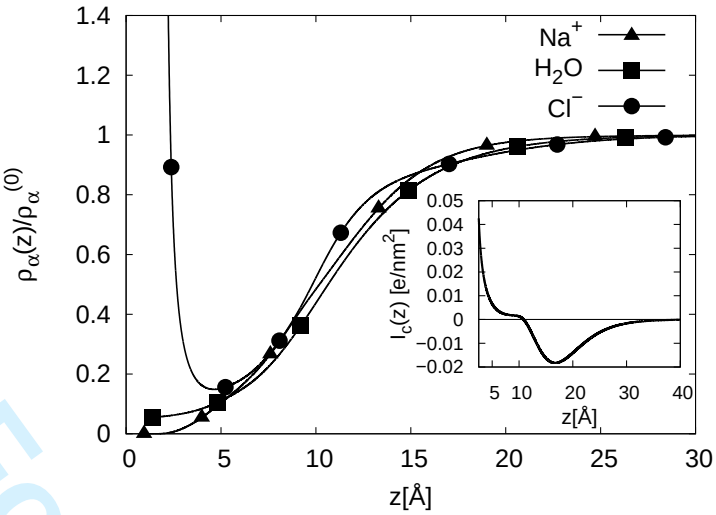

Figure 11: Density profiles of 1M NaCl at liquid-vapour coexistence near a hard wall carrying a surface charge $\sigma = +0.17\,\mathrm{e\,nm^{-2}}$). $\mathrm{T} = 0.769\mathrm{T_c}$, ε is a sigmoidal function defined by (34). The inset shows the total amount of charge per unit area $\mathrm{I_c(z)}$ contained between 0 and z.

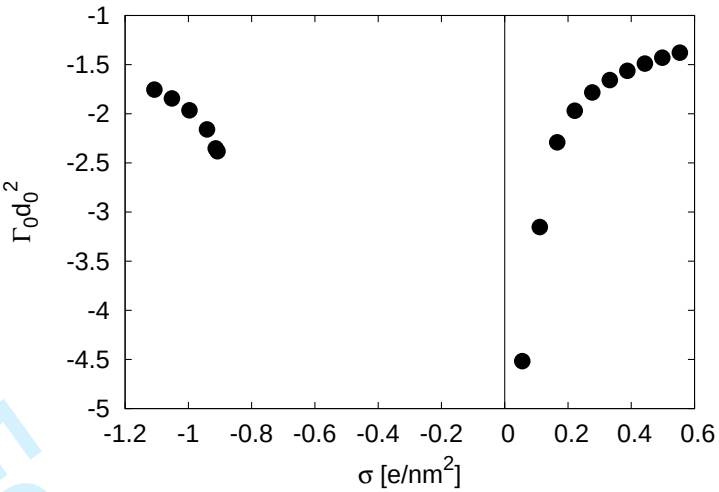

Figure 12: Solvent adsorption of 1M NaCl at liquid-vapour coexistence as a function of substrate surface charge density σ. $\varepsilon(z)$ is given by the CM expression (32), $T = 0.769T_c$.

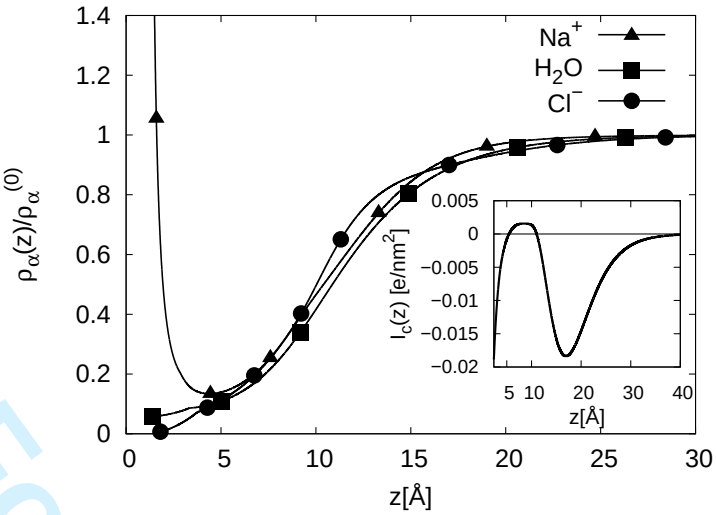

Figure 13: Density profiles of 1M NaCl near a charged hard substrate under liquid-vapour coexistence conditions. $\mathrm{T} = 0.769\mathrm{T_c}$, $\sigma = -0.91\,\mathrm{e/nm^2}$ and the dielectric permittivity is a sigmoidal function of the solvent's density. Inset as in Fig. 11.